Stress relaxation in quasi-two-dimensional self-assembled nanoparticle monolayers

Leandra S. Boucheron,[1] Jacob T. Stanley,[1] Yeling Dai,[1] Siheng Sean You,[2] Christopher T. Parzyck,[1] Suresh Narayanan,[3] Alec R. Sandy,[3] Zhang Jiang,[3] Mati Meron,[2,*] Binhua Lin,[2,†] and Oleg G. Shpyrko[1,‡]

[1]*Department of Physics, University of California San Diego, La Jolla, California 92093, USA*

[2]*James Franck Institute, University of Chicago, Chicago, Illinois 60637, USA*

[3]*Advanced Photon Source, Argonne National Laboratories, Argonne, Illinois 60439, USA*

(Received 29 June 2017; published 11 May 2018)

We experimentally probed the stress relaxation of a monolayer of iron oxide nanoparticles at the water-air interface. Upon drop-casting onto a water surface, the nanoparticles self-assembled into islands of two-dimensional hexagonally close packed crystalline domains surrounded by large voids. When compressed laterally, the voids gradually disappeared as the surface pressure increased. After the compression was stopped, the surface pressure (as measured by a Wilhelmy plate) evolved as a function of the film aging time with three distinct timescales. These aging dynamics were intrinsic to the stressed state built up during the non-equilibrium compression of the film. Utilizing x-ray photon correlation spectroscopy, we measured the characteristic relaxation time (τ) of in-plane nanoparticle motion as a function of the aging time through both second-order and two-time autocorrelation analysis. Compressed and stretched exponential fitting of the intermediate scattering function yielded exponents (β) indicating different relaxation mechanisms of the films under different compression stresses. For a monolayer compressed to a lower surface pressure (between 20 mN/m and 30 mN/m), the relaxation time (τ) decreased continuously as a function of the aging time, as did the fitted exponent, which transitioned from being compressed (>1) to stretched (<1), indicating that the monolayer underwent a stress release through crystalline domain reorganization. However, for a monolayer compressed to a higher surface pressure (around 40 mN/m), the relaxation time increased continuously and the compressed exponent varied very little from a value of 1.6, suggesting that the system may have been highly stressed and jammed. Despite the interesting stress relaxation signatures seen in these samples, the structural ordering of the monolayer remained the same over the sample lifetime, as revealed by grazing incidence x-ray diffraction.

DOI: 10.1103/PhysRevE.97.052803

I. INTRODUCTION

Beginning in the late 1800s, Lord Rayleigh hypothesized from experimental observations that given enough surface area, a droplet of oil spread across water forms a molecular monolayer [1]. Further work by Irving Langmuir and Katharine Blodgett transformed this new field of study from an observational curiosity into a technique for creating and extracting films of monolayer thickness [2,3]. Now, nearly a century later, as technological developments have progressed on increasingly smaller length scales, the Langmuir-Blodgett technique, used to produce and transfer nanoscale thin films, has flourished with further applications and the introduction of engineered nanoparticles [4–18]. These developments have transformed the liquid-air interface into a veritable playground for studies involving states of matter and phase changes in quasi-two-dimensional (quasi-2D) systems.

Recently, great attention has been paid to the structure, ordering, and variety of elastic responses of thin sheets of nanoparticles at the air-water interface in a Langmuir trough [4,5,11,17,19–27]. Upon drop-casting onto the surface of water, monodisperse nanoparticles (<10% polydispersity) self-assemble into islands of two-dimensional (2D) hexagonally close packed crystalline domains surrounded by large voids. When compressed laterally, the voids gradually disappear and the islands merge into a continuous monolayer. Under further compression, these monolayers may buckle, wrinkle, or fold. By treating these monolayers as a piece of a continuous elastic sheet, research has explained satisfactorily the underlying physics of these rich morphological transitions using theories of linear and non-linear elasticity. However, dynamics of these solid 2D sheets on the length scale of individual nanoparticles has yet to be explored.

The behavior of the surface pressure of a 2D particle film as a function of time is usually a sensitive indicator that reveals the underlying complex dynamics. During a compression of a monolayer of nanoparticles, the surface pressure typically undergoes a monotonic increase until the onset of the buckling transitions [5]. If the compression is stopped at any point along the surface pressure-area isotherm, the surface pressure drops precipitously in the first few seconds, followed by slower decays that may last for hours, indicating a non-equilibrium relaxation process [28]. On the other hand, *in situ* Grazing Incidence X-ray Diffraction (GIXD) measurements tend to show that the lattice spacing and domain size of the 2D crystalline structure

*Also at Center for Advanced Radiation Sciences, University of Chicago, Chicago, Illinois 60637, USA.

†Also at Center for Advanced Radiation Sciences, University of Chicago, Chicago, Illinois 60637, USA; lin@cars.uchicago.edu

‡oshpyrko@physics.ucsd.edu

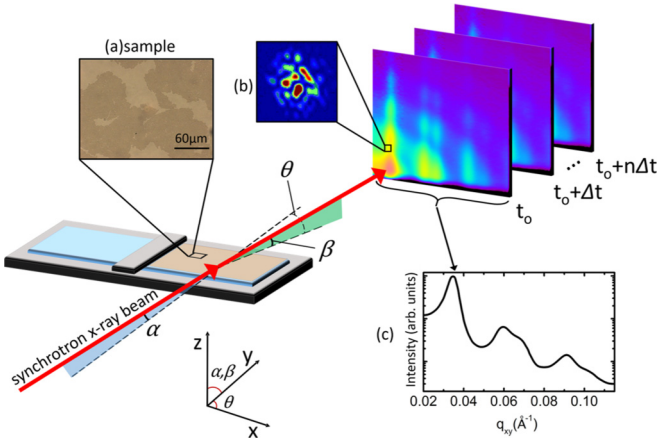

FIG. 1. Geometry of liquid surface scattering setup. XPCS measurements were taken at the position of the first order GIXD peak with (a) inset showing optical microscopy image of uncompressed film (surface pressure ∼4 mN/m), (b) generic speckle pattern measured in XPCS superimposed on GIXD peak, and (c) line integral of 2D diffraction pattern showing first- through fifth-order GIXD peaks.

of the monolayer remain consistent during the slow relaxation process [19]. An open question regards the mechanism through which the nanoparticles release the stress that was built during the compression. Is it released through individual nanoparticle Brownian or non-Brownian diffusion processes, as seen in most of the dense colloid fluid systems, through crystalline domain rearrangement, or through a combination of these mechanisms?

Surface pressure as a function of time following a monotonic step compression has been used widely to study the relaxation dynamics of 2D Langmuir polymeric or nanoparticle thin films [28–32]. Experimental techniques for directly measuring the motions of nanoparticles in nanoparticle monolayers has taken longer to develop than those for measuring the static structure of the same systems. Such studies have become particularly prevalent in recent years due to the substantial increases in both spatial and temporal resolution afforded by coherent x-ray beamlines at synchrotron sources [33]. Along with the ability to study *in situ* dynamics came the capacity to observe processes such as glass formation, relaxation, collective dynamics, and jamming in real time [7,34–36]. Recently, X-ray Photon Correlation Spectroscopy (XPCS) has been used to study the diffusion and hydrodynamic interactions of 2D gel systems composed of disordered nanoparticle assemblies at the air-water interface [37–39].

In this work, we examine the effects of macroscale pressure on ordering, stress formation, relaxation, and collective motion of a quasi-2D crystalline system by studying a monolayer of ordered nanoparticles on the surface of water through a combination of surface pressure measurements with both XPCS and GIXD (see Fig. 1). We present some of the first direct measurements of particle dynamics of nanoparticle monolayers at the water-air interface, which bridge a connection between individual nanoscale particle dynamics and macroscopic film structure and dynamics.

II. EXPERIMENTAL METHODS

Langmuir monolayers of iron oxide nanoparticles used in this work consist of organic-soluble spherical iron oxide nanoparticles (Fe_3O_4) (Ocean Nanotech), 20 nm in core diameter with a measured core size distribution of 9.4%. Oleic acid (1.97 nm in length) creates a hydrophobic coating on these particles and prevents aggregation [40]. We suspended the powder form of the nanoparticles as received in chloroform to create a solution with a concentration of 0.5 mg/mL. We drop-cast this solution onto a clean water surface in an 80 cm^2 Langmuir-Blodgett trough. After chloroform evaporation and system equilibration of around an hour, the particles were spread to an approximate surface area coverage of 60%. The width of the trough was 7 cm and the surface area of the trough was varied from 80 cm^2 to a minimum of 35 cm^2 by moving a barrier length-wise (see Fig. 1).

A single KSV Minimicro system 1G microbalance with a Wilhelmy plate (1 cm wide chromatography paper) oriented parallel to the barrier was used to measure the surface pressure, Π, of the monolayer ($\Pi = \gamma_0 - \gamma$, where γ_0 and γ are the surface tension of the water and the monolayer, respectively). We monitored the in-plane surface pressure for the duration of our XPCS measurements.

As an important note, for most nanoparticle monolayers, the value of the surface pressure depends on the orientation of the Wilhelmy plate relative to the direction of the compression of the monolayers, a phenomenon known as "surface pressure anisotropy". You *et al.*, reported on a study of the surface pressure anisotropy of a Langmuir monolayer composed of iron oxide nanoparticles (core diameter of 15 nm, Ocean Nanotech) [11]. The measurements were done with two Wilhelmy plates oriented orthogonally to each other; one parallel, $\Pi_{\parallel}$, and one perpendicular, $\Pi_{\perp}$, to the moving barrier. The anisotropy in surface pressure arose because the monolayer exhibited a small but non-zero shear modulus manifested from the uniaxial compress of the monolayer, which is typical of viscoelastic nanoparticle monolayers [41,42]. Nevertheless, the relaxation behaviors measured by the two pressure sensors were very similar qualitatively.

Following sample deposition and equilibration, we laterally compressed our films at a continuous, constant compression rate of 1 cm^2/min to a target surface pressure of 20 mN/m, 30 mN/m, or 40 mN/m, respectively, for separate samples, fixed the barrier in position, and allowed the film to relax (i.e., "age"). We called this the point where the aging time, $t_a = 0$, corresponding to the time at which we began dynamics measurements (see Figs. 3 and 4). We verified via x-ray reflectivity that all of the iron oxide films were monolayers in these pressure regimes.

X-ray scattering measurements were carried out at the Advanced Photon Source (APS); the dynamic XPCS experiments were performed at beamline 8-ID-I, and the static GIXD measurements were taken at ChemMatCARS beamline 15-ID-C. Specifics on the beamline optics and beam coherence of 8-ID-I are presented elsewhere [43]. The experimental set-up was placed in reflection geometry (Fig. 1) with an angle of incidence of $\alpha = 0.14^{\circ}$, below the critical angle for water at an incident x-ray beam energy of 7.35 keV. The sample-detector

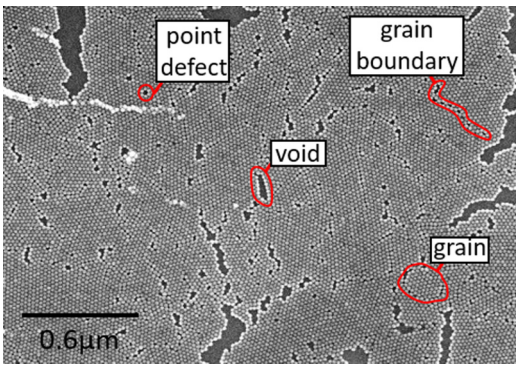

FIG. 2. SEM image of nanoparticle film transferred to silicon substrate via Langmuir-Schaefer transfer method. Grains represent regions of relatively uninterrupted hexagonally close packed nanoparticles, separated by grain boundaries along which the close packing is not observed. These grains are punctuated by point defects, where a single or a few particles are missing from the otherwise crystalline arrangement. Voids are empty regions in between the grains. The presence of these artifacts suggests polycrystalline behavior.

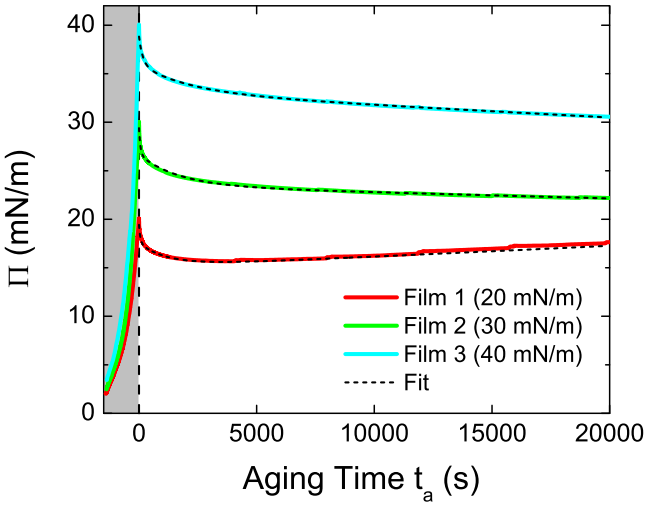

FIG. 3. Surface pressure (Π) measurements and fits (see Table I) for three different iron oxide thin films. Pressure measurements were taken using a Wilhelmy plate and microbalance, showing reproducible trends.

distance of about 4 m was sufficient to generate x-ray speckle on the order of the pixel size to allow for maximal resolution.

XPCS frames were collected every ∼1 s, as dictated by the minimum readout time of the detector (Princeton Instruments), while the maximum time delay (Δt as seen in Figure 5) for a single data set, 2400 s, was determined by considering the combined effects of beam stability and maximum exposure time of the sample. Because the nanoparticles are ligated with organic thiols, the nanoparticles can become sintered and the gold cores can fuse if the film is overexposed to the x-ray beam. Beam stability was determined using a static reference sample, while maximum exposure time was determined by monitoring reflectivity for signs of sample damage. In between measurements, we moved the sample laterally by 40 μm, or twice the beam width, in order to minimize sample damage. Through the subsequent repetition of such measurements, we were able to collect data on the sample for t_a between 10^3 and 10^5 s.

In order to achieve a compromise between signal-to-noise and spatial resolution, we probed our sample over a wave vector range of $0.30\ \mathrm{nm}^{-1} < q_{xy} < 0.36\ \mathrm{nm}^{-1}$, corresponding to the maximum of the static structure factor at $q_{xy,\max} = 0.33\ \mathrm{nm}^{-1}$ (first order GIXD peak) for a center-to-center particle distance, a, of $a = 2\pi/(q_{xy}\sin(60^\circ)) = 22$ nm. Due to limited scattering intensity, this q-range was not large enough for us to observe a consistently measurable q-dependence of the timescale in the XPCS measurements, so the timescale measurements presented in this manuscript were calculated from scattering data extracted from the middle of the q-range, with a width of $0.0025\ \mathrm{nm}^{-1}$. Second-order intensity autocorrelation functions were calculated using XPCSGUI software designed for sector 8-ID at APS.

III. RESULTS AND DISCUSSION

Figure 2 shows a scanning electron microscopy (SEM) image of one of our compressed 20 nm iron oxide monolayers at a surface pressure of about 20 mN/m that we transferred from the liquid surface onto a silicon substrate using the Langmuir-Schaefer technique. This image shows the existence of voids, grain boundaries, and crystalline point defects formed in the compressed films, indicating a highly complex granular system.

Stanley *et al.* reported in a previous study of the same nanoparticle system that the structural information obtained from the analysis of the first through fifth order GIXD Bragg peaks from the monolayer on the surface of water is in good agreement with that obtained from the analysis of the SEM image of the transferred monolayer on the silicon substrate [22]. Both methods yielded the same center-to-center particle spacing and correlation length of about 15 particle separations [23]. We infer from this result that the transferring process preserves the essential crystalline domain structure shown in Fig. 2.

We studied the dynamics of the stress relaxation of the nanoparticle monolayers with pressure sensor measurements in the Langmuir trough and XPCS simultaneously as the film aged; the former measured macroscopic behavior of the monolayer across the entire trough whereas the latter measured microscopic particle dynamics at the length scale of individual nanoparticles.

We first examine the results using the Langmuir trough method and discuss the dynamics of a compressed monolayer characterized by the behavior of the surface pressure after the compression was stopped at a given target pressure. Surface pressure was recorded continuously as a function of the aging time, t_a. Figure 3 shows the t_a-dependent surface pressure curves for three different monolayers compressed to three different target pressures. When the first film was compressed to a target pressure of 20 mN/m (Film 1), the surface pressure showed an initial sharp drop within the first 100 s, followed by a slower decay to about 1000 s, and then a very slow increase during the remaining time. For the second and third films with target pressures of 30 mN/m (Film 2) and 40 mN/m (Film 3), the surface pressure showed similar behavior to Film 1 during the first 1000 s, followed by a very slow decay. These results

TABLE I. The pressure curves following $t_a = 0$ shown in Fig. 3 were fit to the form $\Pi(t) = ae^{-\frac{t}{t_1}} + be^{-\frac{t}{t_2}} + ce^{-\frac{t}{t_3}}$ with parameters as follows. t_3 for Film 1 is negative, corresponding to the long-timescale increase in Π.

	a	t_1 (s)	b	t_2 (s)	c	t_3 (s)
Film 1	1.88	90	2.44	1.2×10^3	15.1	-1.3×10^5
Film 2	2.74	60	3.22	1.7×10^3	23.4	3.5×10^5
Film 3	2.85	160	2.84	2.1×10^3	33.1	2.4×10^5

indicate that the compression process creates defects and point stresses that are able to relax and rearrange once the barrier is fixed in position and film surface area is held constant, and we will discuss this possibility later in conjunction with XPCS measurements.

The surface pressure-time curves can be fit well by a linear combination of three exponential functions, with the fitted time constants revealing characteristic dynamics in three distinct aging time regions of $t_1 \sim 10^2$ s, $t_2 \sim 10^3$ s, and $t_3 \sim 10^5$ s, respectively, as shown in Table I. Surface pressure measurements cannot be taken for longer aging times, as water evaporation from the trough begins to have a significant impact on film structure over a timescale of several hours. All of our measurements have shown that the pressure never reaches an equilibrium value within the measured timescales.

Over the lifetime of each film, the center-to-center particle spacing, measured to be 22 nm at $\sim t_a = 0$, changed by less than 2 Å, or 1% of the particle size, as determined by the location of the GIXD peak. Similarly, the coherent length of about 15 particle diameters varied by less than 15%, or fewer than two particles, in all cases, as determined by the width of the GIXD peak. The slow decay of the surface pressure following the initial drop, combined with the consistency of the structure factor, seem to indicate that the particle ordering within the 2D crystalline domains of the films quickly reached a metastable state.

An exponential decay of a stress (pressure) as a function of time, e^{-t/t_0}, is commonly observed in simple viscoelastic materials relaxing at a constant strain (area or volume). This stress-time dependence can be explained by the so-called "Maxwell model", in which the viscoelastic property is represented by a purely viscous damper (viscosity of η) and a purely elastic spring (elastic modulus of E) connected in series ($t_0 = \eta/E$) [44]. For more complex materials in which there may exist multiple mechanisms of relaxation dynamics, such as in nanoparticle or polymer thin films, the surface pressure can no longer be fit with a simple exponential. Instead, stretched exponentials [30] and multi-exponentials [28,32] have been used to model the time-dependent pressure curves to explain the complex dynamics of these out-of-equilibrium thin films.

Based solely on the response function of the surface pressure after compression of the films, we hypothesize that the films undergo a fast elastic response in the time region of t_1, followed by a slower damping of viscous surface fluctuations in the region of t_2, and finally reach a metastable state at the long time region of t_3. Particularly relevant to our research was the study of a Langmuir monolayer of 2D gels composed of polydisperse silica nanoparticles assemblies [32], in which the polydispersity of the nanoparticles generally led to a gel-like 2D structure. In this study, the relaxation of the parallel pressure, $\Pi_\parallel$, curve at higher pressures was also fit by a linear combination of three exponentials, characterized by three time constants: t_1 and $t_2 \sim 10^2$ s and $t_3 \sim 10^3$ s. Three different relaxation processes were proposed: 1) damping of surface fluctuations, 2) rearrangement of particle rafts, and 3) particle motion inside the raft, which indicates that the dynamics of a gel-like monolayer are much faster than that of a 2D crystalline monolayer.

With the three distinct time regions displayed in the macroscopic surface pressure-time curves, characterized by t_1, t_2, and t_3, we now examine the results of XPCS measurements to gain insight into the microscopic nanoparticle movement that is linked to the behavior of the surface pressure in each of these time regions, which, to our knowledge, is the first application of XPCS to a quasi-2D crystalline structure supported on a liquid surface.

To gain information on nanoparticle dynamics, it is useful to analyze the second order intensity autocorrelation function, which is determined according to the formula

$$g_2(\Delta t) = \frac{\langle I(t)I(t+\Delta t)\rangle_t}{\langle I(t)\rangle_t^2} \tag{1}$$

and fit to the form

$$g_2(\Delta t) - 1 = b\left[e^{-\left(\frac{\Delta t}{\tau}\right)^\beta}\right]^2 = b[g_1(\Delta t)]^2, \tag{2}$$

where $I(t)$ is the beam intensity, Δt is the variable time delay, b is the Siegert factor, τ is the characteristic relaxation time, g_1 is the first-order field autocorrelation function, and β is the stretched or compressed exponent. The relaxation times, τ, were calculated for each of the samples by fitting the exponent β using a non-linear least squares algorithm.

Figure 4(a) shows the relaxation time, τ, for all three films throughout the same aging process as the surface pressures recorded in Fig. 3. For both Films 1 and 2, τ decreases over all three time regions. Film 3 shows the opposite behavior, with τ increasing in the first (t_1) and second (t_2) time regions and gradually leveling off in the long aging-time region (t_3).

Figure 4(b) plots the results of the fitted exponent β for all three films, along with guides to the eye (solid lines) to elucidate the underlying trends. As the target surface pressure on the film increases, so does the average value of β. In the cases of Films 1 and 2 (20 mN/m and 30 mN/m, respectively), β undergoes a significant drop, changing from a compressed exponent during the first two time regions to a stretched exponent at long timescales. In the case of Film 3 (40 mN/m), on the other hand, the exponent remains compressed, stabilizing around 1.6 after the initial variation between 1.5 and 1.8.

The exponent β in the intensity autocorrelation function has been used to identify different stress relaxation processes in viscoelastic materials, with $0 < \beta < 1$ (stretched) indicating a glassy system, $\beta = 1$ indicating Brownian diffusion, and $\beta > 1$ (compressed) indicating a system with local or microscopic stresses [45,46]. For Films 1 and 2, the behavior of the exponent β suggests a large-scale stress release into a glassy state through crystalline domain redistribution, possibly through domain re-orientation and translational motions [47], whereas the result for Film 3 suggests that under higher surface

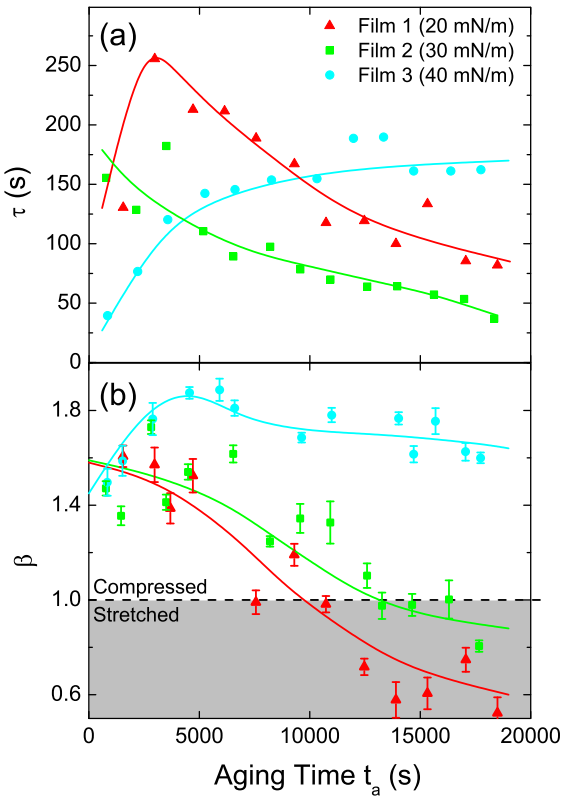

FIG. 4. (a) Characteristic relaxation time (τ) measurements as a function of aging time for iron oxide thin films. Relaxation time measurements were calculated using XPCS technique. Solid symbols represent data; solid lines are guides to the eye to reveal overall trends. (b) Stretched or compressed exponent (β) as a function of film age for three different films. Solid symbols represent data; solid lines are guides to the eye. The average exponent increases as initial film pressure increases. Films 1 and 2 show a transition from compressed to stretched exponent as the film ages. Film 3 shows the most constant exponent, indicating little change in its overall stresses.

pressures the film is highly stressed with local rearrangements or defect reorganization but no bulk glass transition, as β remains consistently compressed.

We now take a closer look at Film 3, for which the exponent is compressed ($\sim$1.6) and most constant. Although structure factor measurements point towards a quasi-static system after the initial pressure drop, it is clear from the behavior of the relaxation time τ and exponent β that the system exhibits interesting nanoparticle dynamics in this non-equilibrium state. Figure 5 shows the normalized second-order autocorrelation functions, $g_2(\Delta t)$, for Film 3 at varying film ages, with an average Siegert factor of $b = 0.035$. At shorter t_a (<5000 s, in the aging time region of t_2), the relaxation time [Fig. 4(a)] increased dramatically before roughly leveling off at longer t_a. This behavior is indicative of aging in the system as the particle dynamics slows down. Given the q-value at the center of our GIXD range of 0.33 nm^{-1} and an approximate τ of 200 s, as shown in Fig. 4(a), particles would diffuse roughly at a rate of $v = 1/\tau q = 0.015$ nm/s, and would thus traverse an approximate distance of 3 nm through undirected motion during τ of 200 s. This length scale is a fraction of the observed grain size of the nanoparticle domains (approximately 200 nm

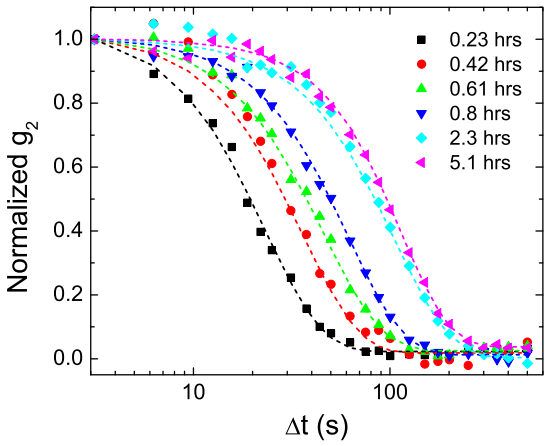

FIG. 5. Normalized second order autocorrelation function g_2 for selected film ages of Film 3 at wave vector transfer $q = 0.33$ nm^{-1}. Dashed lines are the result of fits to Eq. (2).

across, as calculated by the width of the GIXD peak). The behavior of β for Film 3 also indicates unusual non-Brownian particle dynamics. As shown in Fig. 4(b), β increases from a value of 1.5 to around 1.8, and then levels off around 1.6 at a longer aging time region of t_3, where $\beta = 1.5$ is commonly found in three-dimensional jammed soft matter systems [48–51].

For Film 3, we also employed the two-time intensity autocorrelation function given by

$$g_{2,2-\text{time}}(\Delta t_1, \Delta t_2) = \frac{\langle I(t+\Delta t_1) I(t+\Delta t_2)\rangle_t}{\langle I(t)\rangle_t^2}, \qquad (3)$$

where Δt_1 and Δt_2 are two time delays encompassing the same time range. The results are shown in Fig. 6. As the film ages, the relaxation time, τ, increases on average, as shown by the width of the high-intensity region. However, the inset shows a representative point at which the two-time autocorrelation function pinches off. This shape is a signature of a local avalanche that causes sudden stress release from a blockage, suggesting a discontinuous rearrangement of particles in a non-equilibrium heterogeneous jammed system [52]. We verified that this sudden change in the two-time correlation is not due to variable beam intensity or experimental artifacts, and is visible at all measured q-values, meaning that the rearrangement happened across a range of length scales.

When combined with the results from SEM imaging (Fig. 2), reciprocal space GIXD, and the dynamic surface pressure measurements (Fig. 3), the results from XPCS measurements suggest different mechanisms of particle dynamics in distinct aging time regions, as illustrated in the schematics in Fig. 7. We infer that the nanoparticles self-assembled into 2D crystalline domains upon spreading at the air-water interface, with crystalline domains relatively far apart [Fig. 7(a), stage 1]. As the film was compressed laterally, the crystalline domains gathered closer into contact [stages 2–3 in Figs. 7(b) and 7(c)], forming a macroscopically continuous sheet with grain boundaries, point defects, and a small number of voids [stage 4 in Fig. 7(d)]. The aging dynamics after the compression was stopped were intrinsic to the stressed state built up during the non-equilibrium compression of the film. Because the exponent, β, is either smaller (stretched) or larger (compressed) than

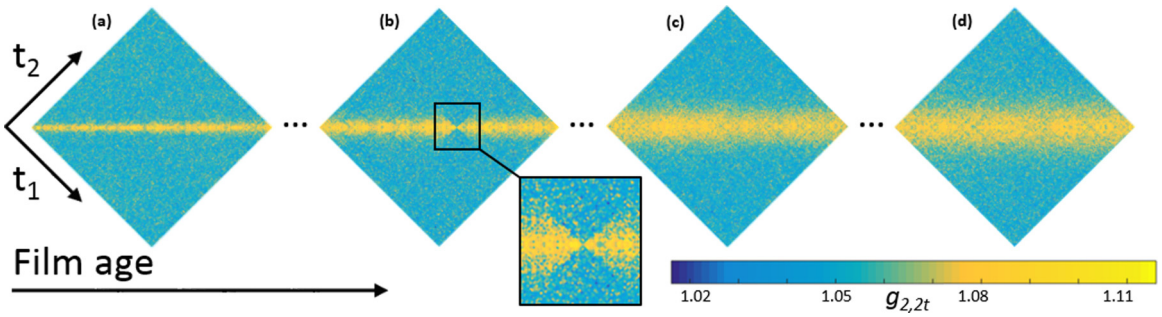

FIG. 6. Color map of two-time autocorrelation for various film ages of (a) 0.23–0.42 h, (b) 0.61–0.80 h, (c) 1.3–1.5 h, (d) 3.9–4.1 h. Inset shows a pinch point corresponding to a dramatic structural rearrangement of the probed sample region.

1, the particle motion was non-Brownian in nature; the particles inside the crystalline domains could only vibrate around the lattice point, with the particles lining the grain boundaries moving very slowly. When the compression was stopped at a lower or intermediate surface pressure (stages 2–3), as in the case of Films 1 and 2, the domains may have redistributed to release the stress through shearing and rotating [Fig. 7(e)] [53]. However, if the compression was stopped at a higher pressure (stage 4), as in the case of Film 3, where the crystalline domains were locked in place, the particle dynamics were limited to the grain boundaries, with collective motions of the nanoparticles along the grain boundaries, as depicted in Fig. 7(f) [6,21]. We suspect that in this highly stressed state, the nanoparticles were jammed along the grain boundaries, and hence, a localized relaxation could induce a sudden stress release, which would give rise to the pinches observed in the two-time correlation function shown in Fig. 6.

Returning to the characteristic relaxation time measurements seen in Fig. 4, we note that for small values of the aging time, during which all of the films underwent a rapid change in surface pressure (Fig. 3), it is likely that the films exhibited significant spatial heterogeneity. We also point out that all three films experienced an increase in relaxation time for a film aging time around 3000–4000 s, indicating a period of time during which the dynamics slowed. However, in the case of Films 1 and 2, the timescale decreased following this point, indicating that any local stresses that may have built up likely had room to undergo major structural rearrangements, as seen in Fig. 7(e). On the other hand, in the case of Film 3, the timescale continued to increase for the duration of the film aging time, indicating a consistently jammed state without the possibility of large-scale rearrangement. The interpretation that the local stresses continued to grow in Film 3 is further supported by the pinch-off point seen in Fig. 6, indicating that while the dynamics timescale underwent a sudden drop due to a local rearrangement [likely along grain boundaries, as seen in Fig. 7(f)], it abruptly returned to its prior value and continued its trend of increasing as a function of film aging time. In the case of Films 1 and 2, however, any such early timescale rearrangement may have had a longer range impact, such that the timescale was able to continue its decreasing trend. We conclude that while stresses exist from the compression process in all of our films, these stresses appear to easily relax for lower surface pressures (20–30 mN/m) while they remain at higher surface pressures (40 mN/m).

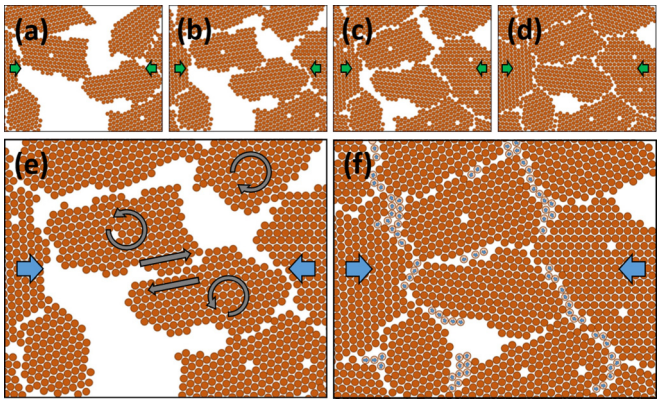

FIG. 7. Schematics of the domain structure of a nanoparticle film compressed laterally to different stages: upon spreading at stage 1 (a), lower surface pressure at stage 2 (b), intermediate surface pressure at stage 3 (c), and higher surface pressure at stage 4 (d). In (a)–(d), the green arrows indicate the direction of active compression. Possible relaxation mechanisms for the particle domains after the compression is stopped are shown for Films 1 and 2 (e), and for Film 3 (f). In (e),(f), the blue arrows indicate the direction of stress due to prior compression.

IV. CONCLUSION

We have presented evidence of different stress relaxation mechanisms in quasi-2D nanoparticle monolayer thin films under a variety of lateral compression pressures. At lower surface pressures, the monolayers underwent a large-scale redistribution of crystalline domains to relieve the stresses in the film, while under higher surface pressures, the films appeared highly stressed and exhibited small avalanches, suggesting that the dynamics were confined to grain boundaries. In all cases, both the overall ordering and the structure factor remained unchanged. Our results represent the first XPCS measurements of particle motion on a quasi-2D crystalline system at the liquid-air interface. While our conclusions may vary depending on the chemical makeup of the nanoparticles and their associated ligands, our experiments suggest a method for further characterization as we have shown that it is possible to directly measure nanoparticle dynamics, including abrupt events, in liquid-air interface monolayers. Future directions could include varying the ligand concentration to measure its effect on the degree of stress relaxation [54]. Additionally, while our work has focused on XPCS measurements perpendicular to the applied stress, further insight into the behavior of the system could be

provided by measurements of the films in multiple orientations. Such monolayers represent a complex system that merits further study for potential uses in engineering and technological applications.

ACKNOWLEDGMENTS

The authors thank the NSF for support under CAREER Award No. DMR-0956131. This research used resources of the Advanced Photon Source, a US Department of Energy (DOE) Office of Science User Facility operated for the DOE Office of Science by Argonne National Laboratory under Contract No. DE-AC02-06CH11357. ChemMatCARS Sector 15 is supported by the NSF under Grant No. NSF/CHE-1346572. B.L. and S.S.Y. thank the NSF for support under Grant No. NSF/DMR-1420709 through the University of Chicago MRSEC.

[1] J. W. S. Rayleigh, The London, Edinburgh, and Dublin Philosophical Magazine **48**, 321 (1899).
[2] I. Langmuir, J. Am. Chem. Soc. **39**, 1848 (1917).
[3] M. C. Petty, *Langmuir-Blodgett Films: An Introduction* (Cambridge University Press, New York, 1996).
[4] Y. Dai, B. Lin, M. Meron, K. Kim, B. Leahy, and O. G. Shpyrko, J. Appl. Phys. **110**, 102213 (2011).
[5] B. D. Leahy, L. Pocivavsek, M. Meron, K. L. Lam, D. Salas, P. J. Viccaro, KaYee C. Lee, and B. Lin, Phys. Rev. Lett. **105**, 058301 (2010).
[6] K. Schwenke, L. Isa, and E. Del Gado, Langmuir **30**, 3069 (2014).
[7] J. W. Swan, J. L. Bauer, Y. Liu, and E. M. Furst, Soft Matter **10**, 1102 (2014).
[8] K. Chokprasombat, C. Sirisathitkul, and P. Ratphonsan, Surf. Sci. **621**, 162 (2014).
[9] J. B. Edel, A. A. Kornyshev, and M. Urbakh, ACS nano **7**, 9526 (2013).
[10] C. Y. Lau, H. Duan, F. Wang, C. B. He, H. Y. Low, and J. K. W. Yang, Langmuir **27**, 3355 (2011).
[11] S. S. You, R. Rashkov, P. Kanjanaboos, I. Calderon, M. Meron, H. M. Jaeger, and B. Lin, Langmuir **29**, 11751 (2013).
[12] S. Kinge, M. Crego-Calama, and D. N. Reinhoudt, Chem. Phys. Chem. **9**, 20 (2008).
[13] S. C. Glotzer, M. J. Solomon, and N. A. Kotov, AIChE J. **50**, 2978 (2004).
[14] B. A. Grzybowski, C. E. Wilmer, J. Kim, K. P. Browne, and K. J. M. Bishop, Soft Matter **5**, 1110 (2009).
[15] M. Grzelczak, J. Vermant, E. M. Furst, and L. M. Liz-Marzán, ACS nano **4**, 3591 (2010).
[16] D. Mishra, M. J. Benitez, O. Petracic, G. A. Badini Confalonieri, P. Szary, F. Brussing, K. Theis-Brohl, A. Devishvili, A. Vorobiev, O. Konovalov *et al.*, Nanotechnology **23**, 055707 (2012).
[17] A. Böker, J. He, T. Emrick, and T. P. Russell, Soft Matter **3**, 1231 (2007).
[18] A. Ulman, Chem. Rev. **96**, 1533 (1996).
[19] D. G. Schultz, X.-M. Lin, D. Li, J. Gebhardt, M. Meron, P. J. Viccaro, and B. Lin, J. Phys. Chem. B **110**, 24522 (2006).
[20] L. Pocivavsek, R. Dellsy, A. Kern, S. Johnson, B. Lin, K. Y. C. Lee, and E. Cerda, Science (NY) **320**, 912 (2008).
[21] Y. Dai, B. Lin, M. Meron, K. Kim, B. Leahy, T. A. Witten, and O. G. Shpyrko, Langmuir **29**, 14050 (2013).
[22] J. Stanley, Y. Dai, L. Boucheron, B. Lin, M. Meron, and O. Shpyrko, Rev. Sci. Instrum. **86**, 063704 (2015).
[23] J. Stanley, L. Boucheron, B. Lin, M. Meron, and O. Shpyrko, Appl. Phys. Lett. **106**, 161602 (2015).
[24] M. K. Sanyal, S. K. Sinha, K. G. Huang, and B. M. Ocko, Phys. Rev. Lett. **66**, 628 (1991).
[25] M. K. Bera, M. K. Sanyal, S. Pal, J. Daillant, A. Datta, G. U. Kulkarni, D. Luzet, and O. Konovalov, Europhys. Lett. **78**, 56003 (2007).
[26] R. Banerjee, M. K. Sanyal, M. K. Bera, A. Singh, J. Novak, and O. Konovalov, Phys. Rev. E **83**, 051605 (2011).
[27] Y. Lin, A. Böker, H. Skaff, D. J. Cookson, A. Dinsmore, T. Emrick, and T. P. Russell, Langmuir **21**, 191 (2005).
[28] D. Y. Zang, E. Rio, D. Langevin, B. Wei, and B. P. Binks, Eur. Phys. J. E **31**, 125 (2010).
[29] F. Monroy, H. M. Hilles, F. Ortega, and R. G. Rubio, Phys. Rev. Lett. **91**, 268302 (2003).
[30] H. M. Hilles, F. Ortega, R. G. Rubio, and F. Monroy, Phys. Rev. Lett. **92**, 255503 (2004).
[31] H. Hilles, A. Maestro, F. Monroy, F. Ortega, R. G. Rubio, and M. G. Velarde, J. Chem. Phys. **126**, 1 (2007).
[32] Z. DuYang and Z. YongJian, Science China **54**, 1587 (2011).
[33] D. H. Bilderback, P. Elleaume, and E. Weckert, J. Phys. B **38**, S773 (2005).
[34] L. Cipelletti and L. Ramos, J. Phys.: Condens. Matter **17**, R253 (2005).
[35] A. Amir, Y. Oreg, and Y. Imry, Proc. Natl. Acad. Sci. USA **109**, 1850 (2012).
[36] S. Whitelam, E. H. Feng, M. F. Hagan, and P. L. Geissler, Soft Matter **5**, 1251 (2009).
[37] D. Orsi, T. Rimoldi, E. Guzman, L. Liggieri, F. Ravera, B. Ruta, and L. Cristofolini, Langmuir **32**, 4868 (2016).
[38] D. Orsi, A. Fluerasu, A. Moussaïd, F. Zontone, L. Cristofolini, and A. Madsen, Phys. Rev. E **85**, 011402 (2012).
[39] D. Orsi, L. Cristofolini, G. Baldi, and A. Madsen, Phys. Rev. Lett. **108**, 105701 (2012).
[40] H. Duan, M. Kuang, X. Wang, Y. A. Wang, H. Mao, and S. Nie, J. Phys. Chem. C **112**, 8127 (2008).
[41] Z. Jiang, X.-M. Lin, M. Sprung, S. Narayanan, and J. Wang, Nano Lett. **10**, 799 (2010).
[42] Z. Jiang, D. R. Lee, S. Narayanan, J. Wang, and S. K. Sinha, Phys. Rev. B **84**, 075440 (2011).
[43] D. Lumma, L. B. Lurio, M. A. Borthwick, P. Falus, and S. G. J. Mochrie, Phys. Rev. E **62**, 8258 (2000).
[44] R. M. Christensen, *Theory of Viscoelasticity: An Introduction* (Academic Press, New York, 1971).
[45] *Soft Matter Characterization*, edited by R. Borsali and R. Pecora (Springer Netherlands, Dordrecht, 2008).
[46] P. Falus, M. A. Borthwick, S. Narayanan, A. R. Sandy, and S. G. J. Mochrie, Phys. Rev. Lett. **97**, 066102 (2006).

[47] R. Mari, F. Krzakala, and J. Kurchan, Phys. Rev. Lett. **103**, 025701 (2009).
[48] L. Cipelletti, S. Manley, R. C. Ball, and D. A. Weitz, Phys. Rev. Lett. **84**, 2275 (2000).
[49] L. Cipelletti, L. Ramos, S. Manley, E. Pitard, D. A. Weitz, E. E. Pashkovski, and M. Johansson, Faraday Discuss. **123**, 237 (2003).
[50] J.-P. Bouchaud and E. Pitard, Eur. Phys. J. E **6**, 231 (2001).
[51] O. G. Shpyrko, J. Synchrotron Radiat. **21**, 1057 (2014).
[52] C. Sanborn, K. F. Ludwig, M. C. Rogers, and M. Sutton, Phys. Rev. Lett. **107**, 015702 (2011).
[53] J. Jalkanen, G. Rossi, O. Trushin, E. Granato, T. Ala-Nissila, and S. C. Ying, Phys. Rev. B **81**, 041412 (2010).
[54] S. D. Griesemer, S. S. You, P. Kanjanaboos, M. Calabro, H. M. Jaeger, S. A. Rice, and B. Lin, Soft Matter **13**, 3125 (2017).